Nanoscale

ROYAL SOCIETY OF CHEMISTRY

PAPER

View Article Online
View Journal | View Issue

Cite this: *Nanoscale*, 2024, **16**, 3510

Microwave-assisted ZnO-decorated carbon urchin resembling 'shish-kebab' morphology with self-healing and enhanced electromagnetic shielding properties†

Sandeep Kumar Singh, *‡ Rishi Raj,‡ Akshay Sunil Salvi, Sampath Parasuram, S. Kumar and Suryasarathi Bose *

Herein, inspired by *Acacia auriculiformis* fruit, the shish-kebab-like growth of ZnO on carbon urchin (ZnO@CU) was designed using microwave radiation, thus leading to a hierarchal 3D structure that can promote multiple internal reflections through polarization centers. This hierarchal structure was then dispersed in a designer polyetherimide (PEI) matrix containing dynamic covalent bonds that can undergo metathesis, triggered by temperature, to harness self-healing properties in the composite. Such key attributes are required for their potential use in EMI shielding applications where frequent repairs are indispensable. Morphological investigation revealed that the ZnO flower was periodically nucleated like 'shish-kebab' structures on CU surfaces. CU was designed from short carbon fibers using a facile modified method. The EMI shielding performance of the resulting composites was investigated in the X-band, illustrating a shielding effectiveness of −40.6 dB for 2 wt% of ZnO@CU loading, and the composite can be preserved after the self-healing procedure. The ZnO 'kebabs' on 'CU shish' facilitated multiple scattering and numerous polarization centers to improve the EMI shielding performances at extremely low filler contents. In addition, the mechanical and thermal properties of the composite showed improved structural integrity and superior resistance to extreme temperatures, respectively. Overall, the proposed ZnO@CU/PEI composite has great potential to fulfill the increasing demands for lightweight EMI shielding materials in many fields.

Received 13th November 2023,
Accepted 31st December 2023

DOI: 10.1039/d3nr05758e

rsc.li/nanoscale

1. Introduction

Owing to the surprising rapid growth in the electronic and telecommunication industries, the demand for lightweight and thermally stable electromagnetic interference (EMI) shields has massively increased.[1–10] However, the high density of miniaturized devices in these sectors is generating serious electromagnetic (EM) radiation and deteriorating the smooth functioning of devices.[1,11–13] These harmful radiations have become challenging for human health. Consequently, there is a pressing requirement for effective electromagnetic interference (EMI) shielding materials that are capable of interacting with undesired radiation and converting them into heat energy. This capability ensures the protection of both devices and humans from harmful radiation.[14–16]

Carbon allotropes, such as carbon nanotubes (CNTs), graphene, and carbon fibers (CFs), are considered representative EMI shielding materials owing to their low density, high conductivity, and good thermal stability.[1,17–19] Among these, degradable and abundantly sourced fibrous carbon materials, *i.e.* CFs with large specific surface area and lightweight nature, have gained much attention in recent times.[1,20–22] Interestingly, the bonding states/arrangements of carbon atoms in CF materials control their overall crystallinity. This characteristic is of utmost importance as it significantly affects the electrical, thermal, and mechanical properties of CFs as well as their electromagnetic interference (EMI) shielding performances. Consequently, CFs have emerged as a preferred material in various applications, including aerospace, automotive, and electronics.[4,9,10,14–16,18,21,23] For instance, Lu *et al.* observed that 40 wt% of CFs as a filler in a composite illustrated −31 dB of shielding effectiveness (SE_T).[24] Mohan and his fellow coworkers achieved −30 dB of SET with 8 wt% of CFs in composites.[18] However, these composites require high CF loadings to achieve significant EMI shielding values, which partly affect the overall structural properties of the composites.[1,2,18] Consequently, research has shifted to modifying prevailing

Department of Materials Engineering, Indian Institute of Science, Bangalore 560012, India. E-mail: sandks86@gmail.com, sbose@iisc.ac.in

†Electronic supplementary information (ESI) available. See DOI: https://doi.org/10.1039/d3nr05758e

‡Authors contributed equally.

materials and finding new 3D hierarchical structures/assemblies for strong shielding applications.[25] In our previous research endeavor, we manufactured a 3D carbon urchin (CU) structure utilizing short carbon fibers (CFs).[1] Furthermore, we implemented a cutting-edge technique involving microwave-assisted growth to synthesize carbon nanofibers (CNFs) over a CU framework. The synthesized CNF@CU with 1.7 wt contents in the PEDOT:PSS aerogel showed remarkable shielding effectiveness. Although the CNF@CU 3D construct showed excellent EMI shielding performance, the controlled growth of CNF on CU was very difficult because the precise size of the nickel catalyst on the CU surface was the most crucial criterion to ensure nanofiber synthesis. Therefore, a simple one-step synthesis method is required to fabricate a CU-based hierarchal 3D construct for EMI shielding performance.

However, the growth of metallic oxides offers great control in terms of their size, shape, and morphological properties. Zinc oxide (ZnO), with a high dielectric constant, can be a potential EMI shielding material, especially at GHz frequencies.[2,12,26–28] Additionally, its large-scale synthesis and facile preparation processes are extremely advantageous owing to their industrial utility. Currently, ZnO-based hybrid materials have gained huge attention. For instance, Singh *et al.* in their recent study presented a ZnO/graphene hybrid 3D composite, which resulted in −38 dB of shielding efficiency.[2] Shayesteh *et al.* achieved a shielding effectiveness of −27.3 dB using 7.5 wt% of ZnO/CNT hierarchal nanohybrid.[29] However, a recent exploration reveals that further structural modifications have led to a significant improvement in existing EMI performance.[30] For example, Han and colleagues discovered a notable enhancement in EMI shielding values by utilizing modified ZnO/C structures in paraffin composites.[31] This enhancement is attributed to the coarse/porous structure of ZnO, which introduces multiple polarization and scattering centers for microwaves. Amidst a surge of new structural modifications, nature-inspired structures are capturing immense allure. Hong *et al.* achieved high EMI shielding properties through the utilization of epiphyte-inspired multifunctional composites.[30] Therefore, the 3D construct utilizing the nature-inspired structures of ZnO in the polymer matrix can be expected to uplift the overall conductivity and dielectric losses of the composite, hence enhancing the EMI shielding performance.

In addition, the inherent high melting point and thermal conductivity of ZnO can provide additional benefits to these composites.[19,32–35] This is extremely crucial in applications where shielding materials encounter a rapid rise in temperatures, *i.e.* in electronic enclosures or power electronic devices. Hence, the thermal stability of the composites ensures their reliability and longevity, making them suitable for a wide range of demanding applications.[33,35]

In addition to their excellent EMI shielding and thermal properties, the robust structural integrity of composites is another substantial feature owing to their practical applications, such as in the aerospace and automotive industries.[1,33,35] Carbon fiber-based polymer composites have already gained widespread attention owing to their high strength through excellent polymer–fiber interaction, thereby enhancing the overall mechanical performance of the composite.[11,18] Moreover, ZnO offers additional sites for interaction with the polymer, providing additional mechanical integrity.[11,36] Hence, composites with ZnO-based carbon fillers are suitable for applications where mechanical robustness is required. Moreover, in recent years, there has been a rising trend of integrating stimuli response materials (*e.g.*, temperature and wind) into EMI shielding composites to address miscellaneous environmental needs.[37,38] One vital function is self-healing capability, allowing concurrent transformation between time and material structure, largely in aerospace applications.[38] Over time, EMI protecting composites often encounter structural defects, resulting in deterioration in their properties. To prolong their lifecycle and durability, polymer composites containing self-healing properties were introduced.[39–45] Recently, Das *et al.* in their pioneer work fabricated self-healable and recyclable multi-layered polymers reinforced with graphene that exhibited high shielding performance (−34.2 dB).[46] Despite being an encouraging strategy, investigations of sustainable and lightweight EMI shielding composites with self-healing functions have not received much attention, offering many opportunities for the improvement of such multifunctional composites.

Based on our understanding, herein, we design an *Acacia auriculiformis fruit* inspired 'shish kebab' type of morphology with ZnO as 'kebab' on CU 'shish' by microwave synthesis route. The as-fabricated ZnO@CU 3D construct displays a homogeneous and periodic growth of ZnO 'kebabs' over CU. The ZnO@CU is then used as a conductive filler and dynamic polyetherimide (PEI) containing di-sulfide bonds as a polymer

Sandeep Kumar Singh

Dr Sandeep Kumar Singh, an esteemed scholar in nanomaterials and polymer nanocomposites, holds a Ph.D. from IIT Kanpur-India and is conducting impactful postdoctoral research at IISc Bangalore. Renowned for pioneering advancements, he excels in synthesizing nanomaterials and polymer foams through innovative CVD and microwave techniques, notably contributing to EMI shielding applications. Dr Singh's prolific career is underscored by a wealth of publications from his Ph.D. and postdoctoral tenure. His deep innovation capability and commitment to advancing materials science position him as a valuable contributor, aligning seamlessly with our journal's dedication to cutting-edge research in the field. We eagerly anticipate his manuscript submission.

matrix to design a self-healing and lightweight EMI shielding composite. Importantly, the ZnO@CU hierarchical structure offers numerous sites for polymer–CU interaction. Hence, improvements in both mechanical and thermal properties are also highly anticipated in composites. These nature-inspired ZnO 'kebabs' can also provide numerous polarization centers and help attenuate the incoming EM radiation through multiple scattering. The EMI shielding effectiveness of the ZnO@CU/PEI composite is investigated thoroughly in the X-band, *i.e.* 8.2–12.4 GHz. The composite with 2 wt% of ZnO@CU loading yielded a −40.6 dB SE. Moreover, the composite exhibited no change in EMI shielding effectiveness after the healing procedure.

2. Experimental

2.1. Materials

Chopped carbon fibres (CFs) of length 6 mm and diameter of 7 μm were provided by SGL Carbon Company-I. 1-Methyl-2-pyrrolidinone (NMP), hexamethylenetetraamine (HMTA, 99%), 4,4′-(4,4′-isopropylidenediphenoxy)bis(phthalic anhydride) (BPADA, 97%), 4,4′-oxydianiline (ODA, 97%) and 4-aminophenyldisulfide (APD) were obtained from Sigma Aldrich. Zinc acetate dihydrate Zn $(CH_3COO)_2{\cdot}2H_2O$, 98.5%, sodium hydroxide pellets (NaOH, 98%), and zinc nitrate hexahydrate Zn $(NO_3)_2{\cdot}6H_2O$, 98%, ethanol and acetone were received from SDFCL-India. Hydrazine hydrate ($H_4N_2{\cdot}H_2O$; 99%), silver nitrate, and all the chemicals were used without further purification.

2.2. Synthesis of self-healable polyetherimide (PEI)

Equimolar dianhydride (BPADA) and diamine (ODA and APD) monomers were used for polymerization. APD containing a dynamic disulfide bond was added to impart self-healing properties in the PEI. In the first step, diamines (ODA and AFD) were added to a round bottom flask containing NMP. After the complete dissolution of the diamines, BPADA was added to the solution. The mixture was stirred for 48 h under an N_2 atmosphere. The step-growth reaction proceeds with the formation of a prepolymer referred to as polyamic acid (PAA). PAA is converted into polyetherimide through an imidization reaction by step-wise heating. The NMP was dried at 80 °C for 8 hours, 120 °C for 4 hours and 150 °C for 2 hours to ensure slow evaporation and avoid blisters in the PAA film. The imidization of polyamic acid was performed at 250 °C for 15 min to obtain PEI. The rearrangements of bonds and condensation reactions lead to the formation of polyetherimide. The reaction scheme for PEI synthesis is depicted in Fig. 1.

2.3. Synthesis of C–U and ZnO-deposited C–U (ZnO@C–U)

CUs were synthesized using a facile solution-based stirring method. 80–100 mg of as-received chopped CF were added in ethanol/acetone (1 : 1 v/v) solution at 50 °C under constant stirring for 1 hour to obtain macro porous 3-D-shaped urchin. After drying for 1 h, CUs were kept at 400 °C in a muffle furnace to burn off the epoxy sizing on the fibers to perform modifications on the bare surface of CF. The CUs were modified by H_2O_2 (30% v/v solution) to increase oxygen containing functional groups onto the CF surface, providing active sites for ZnO.

The seed solution for ZnO coating was prepared in a two-part system with 0.025 M Zn $(CH_3COO)_2{\cdot}2H_2O$ and 0.04 M NaOH in ethanol until a homogeneous solution was formed. The two solutions were mixed, and the CUs were transferred to the seed solution. CUs were kept in the seed solution for the next 24 hours to ensure a maximum amount of seed absorp-

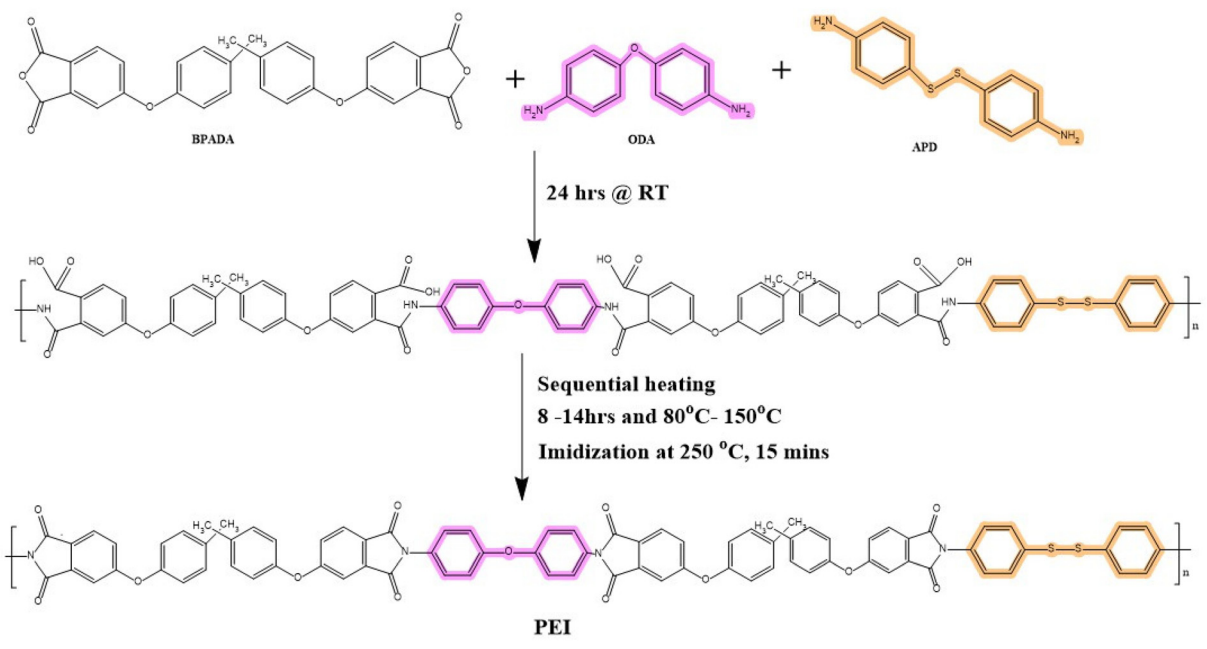

Fig. 1 Reaction scheme and chemical structure of disulfide based polyetherimide.

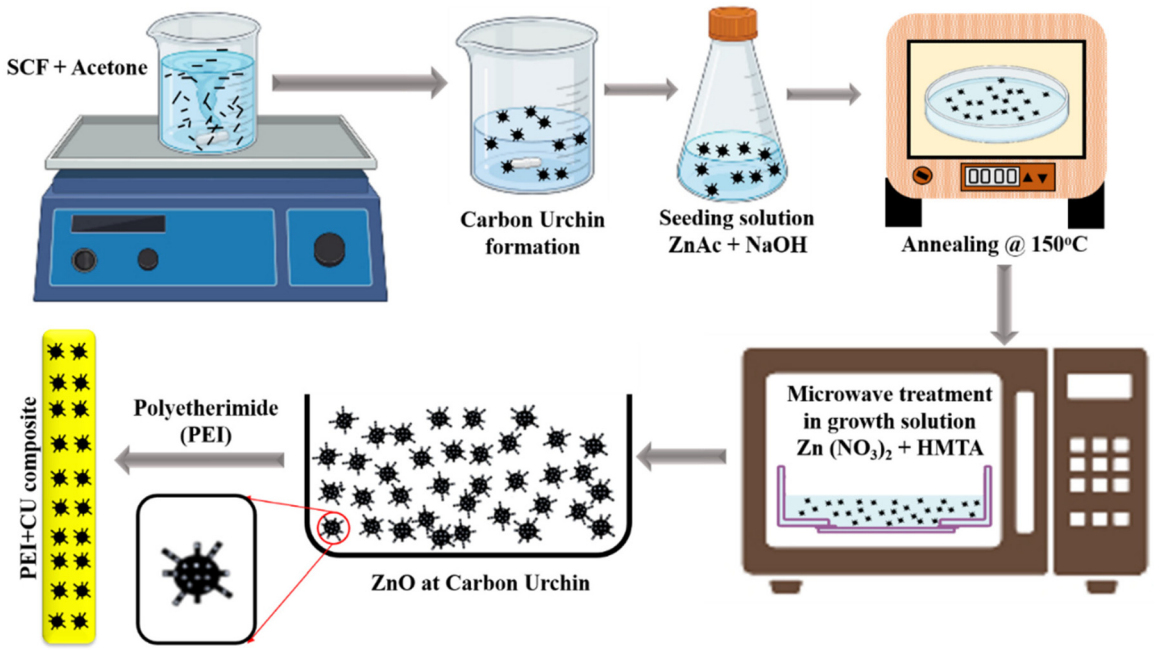

Fig. 2 Process to grow ZnO sheesh-kebab structure on CU.

tion. After seeding, CUs were dried, followed by annealing at 150 °C for 20 min to ensure the fusion of ZnO seeds into the CF surface. The ZnO-seeded CUs are transferred to the growth solution containing a mixture of 0.05 M HMTA and 0.05 M Zn $(NO_3)_2{\cdot}6H_2O$ solution. The growth solution with CUs was irradiated in the microwave at 300 W for 120 seconds, followed by ethanol washing and drying to obtain ZnO@C–U. The representative process is depicted in Fig. 2.

The proposed chemistry for the seeding and growth of ZnO is shown below.[47,48]

ZnO seed layer formation:

$$Zn(CH_3COO)_2 \cdot 2H_2O + 2NaOH \rightarrow Zn(OH)_2 + 2CH_3COO^-Na^+ + 2H_2O$$

$$Zn\ (OH)_2 + 2H_2O \leftrightarrow [Zn(OH)_4]^{2-}$$

$$[Zn\ (OH)_4]^{2-} \leftrightarrow ZnO_2^{2-} + 2H_2O \leftrightarrow ZnO + 2OH^-$$

ZnO growth layer formation:[48,49]

$$C_6H_{12}N_4 + 6H_2O \leftrightarrow 6HCHO + 4NH_3$$

$$NH_3 + H_2O \leftrightarrow NH^{4+} + OH^-$$

$$2OH^- + Zn^{2+} \leftrightarrow Zn\ (OH)_2$$

$$Zn\ (OH)_2 \leftrightarrow ZnO + H_2O$$

2.4. Synthesis of ZnO@CU/PEI composite

The self-healing matrix was initially dissolved in NMP solvent for 10 minutes. Subsequently, the as-synthesized fillers were introduced into the solution, with filler loadings ranging from 0 to 2.0 wt%, resulting in samples designated as PEI, 0.5 ZCUP, 1.0 ZCUP, and 2.0 ZCUP. The solution containing the filler was then transferred into a mold and placed in an oven at 150 °C for 1 hour. Following this, the mold containing the sample was compressed at 20 bar for 1 h while maintaining a temperature of approximately 320 °C.

3. Characterization

X-ray diffraction (XRD) is investigated using XPERT Pro from PANalytical in the 2θ range of 5–80° using CuKα radiation source (λ = 1.5406 Å, 40 kV & 30 mA). The structural information of as-synthesised CU and ZnO-coated CU is taken using a scanning electron microscope (SEM, model-ULTRA 55, bought from Carl Zeiss). Further, elemental analysis of ZnO@CU is completed using energy dispersive X-ray spectroscopy (EDX) that is integrated with FE-SEM. The AC conductivity of ZnO@CU/PEI and PEI composites was studied using an Alpha-A analyzer (Novocontrol, Germany) at room temperature. Thermogravimetric analysis (TGA) of ZnO@CU/PEI and PEI composites is recorded using TA Q500 from TA Instruments by maintaining a heating rate at 10 °C min^{-1} under dynamic nitrogen conditions. The thermal conductivity trends of the composite were studied using a Thermal Conductivity Analyzer: Hotdisk 500S. The study of the mechanical properties of ZnO@C–U/PEI composite was performed using a Dynamic Mechanical Analyzer (Q800, TA instruments, USA) in a single cantilever fixture at an amplitude and frequency of 15 μm and 1 Hz, respectively, from 40 °C to 255 °C at a rate of 3 °C min^{-1}. To study the healing characteristics of

the ZCUP composite, scratches were made using a sharp blade. The ZCUP composite was kept in a hot air oven at 150 °C for 20 min to monitor the healing phenomena. The progress of healing was captured after the duration of 10 min, followed by another duration of 10 min to achieve complete healing.

Finally, the EMI shielding performances are reviewed for ZnO@CU/PEI and PEI composites using keysight (model-field fox microwave analyser N9918A) vector network analyser (VNA) in the X-band (8.2 to 12.4 GHz) at room temperature. The total shielding effectiveness (SE_T), shielding effectiveness from absorption (SE_A) and reflection (SE_R) are calculated using *S*-parameters retrieved during VNA measurement of composites.

The EM radiation that originates from an external device is always eager to perturb the proper functioning of nearby electronic systems. The term EMI shielding effectiveness (SE) is a logarithmic ratio of the input power to the power output, *i.e.* transmitted and typically expressed in decibels (dB). The mathematical expression of SE[1] is

$$SE_{\mathrm{T}} = -10 \log \frac{P_{\mathrm{In}}}{P_{\mathrm{Out}}} \quad (1)$$

where P_{in} and P_{out} are the input and output powers, respectively. Further, when EM wave impinges on the shieling surfaces, they are accompanied by the three mechanisms called absorption (SE_A), reflection (SE_R) and interior multiple reflection (SE_M) presented as follows:[1,13,48]

$$SE_T = SE_A + SE_R + SE_M \quad (2)$$

The SE_A is associated with the dielectric losses of EM waves, SE_R arises owing to impedance mismatch at the air-materials interface and SE_M is a consequence of EM wave multiple reflection within the shielding materials. The third term in eqn (2) is generally neglected when the SE_T exceeds the −10 dB value. Therefore, SE_T in such a situation depends only on reflection and absorption:[1,2]

$$SE_T = SE_A + SE_R \quad (3)$$

Besides, SE_T, SE_R and SE_A can be written as follows:[1,50]

$$SE_{\mathrm{T}} = 10 \log_{10} \frac{1}{|S_{12}|^2} = 10 \log_{10} \frac{1}{|S_{21}|^2} \quad (4)$$

$$SE_{\mathrm{R}} = 10 \log_{10} \frac{1}{\left(1 - |S_{11}|^2\right)} \quad (5)$$

$$SE_{\mathrm{A}} = 10 \log_{10} \frac{1 - |S_{11}|^2}{|S_{21}|^2} = SE_{\mathrm{T}} - SE_{\mathrm{R}} \quad (6)$$

where S_{11}, S_{12}, S_{21}, and S_{22} are the scattering parameters. These scattering parameters are further used to calculate the coefficient of absorption (A), reflection (R) and transmission (T) as follows:[1]

$$R = |S_{11}|^2, T = |S_{21}|^2 \text{ and } A = 1 - R - T \quad (7)$$

4. Results and discussion

4.1. 'Shish-kebab' structures of ZnO@CU

XRD patterns were studied to investigate the presence of ZnO 'kebabs' on CU 'shish' and the crystalline structure of ZnO. The XRD patterns of CU and ZnO@CU are shown in Fig. 3a and b. A strong peak around 26° in Fig. 3a and b clearly reflects the (002) reflection from the graphitic carbon (JCPDS file no. 41-1487).[1,51] As depicted in Fig. 3b, peaks corresponding to ZnO can be observed, representing the successful growth of ZnO over CU. In addition, the peak observed at a 2θ value of 18.5° is attributed to the $Zn(OH)_2$ phase, which is manifested in a limited quantity during the synthesis process. Further, as illustrated in Fig. 3b, the indexed XRD reflection peaks of ZnO@CU indicate a hexagonal wurtzite structure with 3.259 Å of lattice constant and b = 5.216 Å (JCPDS file no. 36-1451).[36]

The SEM images of as-synthesized CU and ZnO@CU are presented in Fig. 4a–e, which are captured at different magnifications. Fig. 4a shows the SEM image of the as-synthesised CU without ZnO. As observed in Fig. 4a and the inset of Fig. 4a,

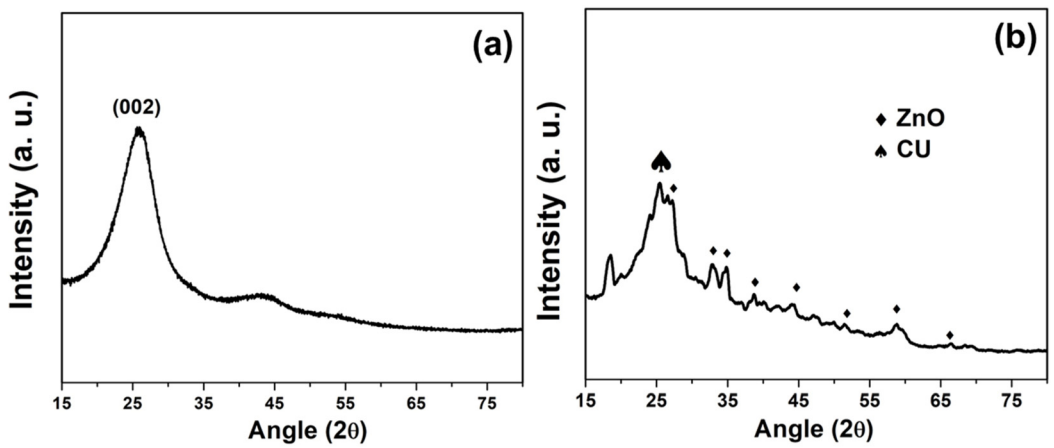

Fig. 3 XRD patterns of (a) as-synthesized CU and (b) ZnO@CU.

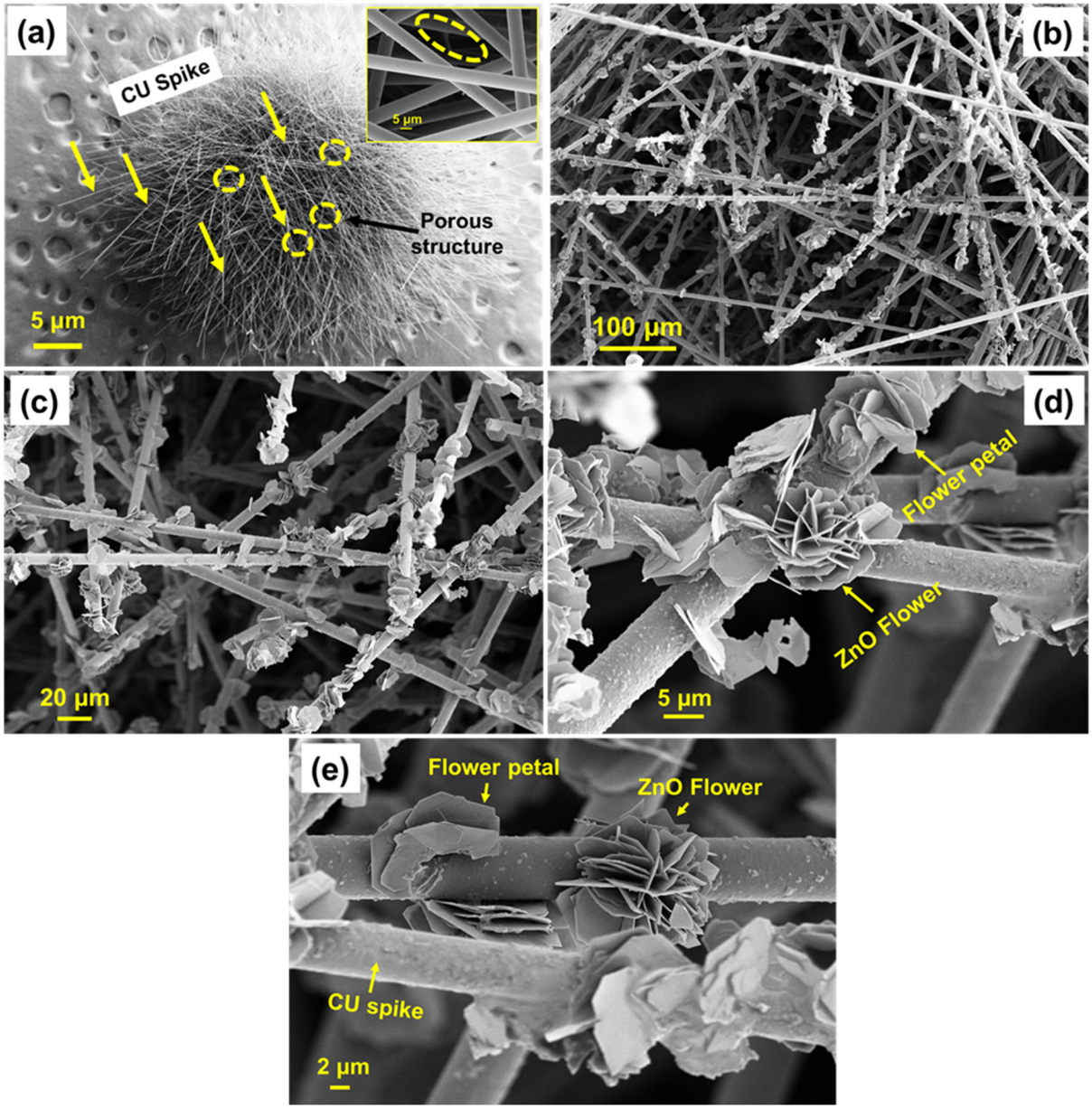

Fig. 4 SEM image of (a) CU and (b)–(e) ZnO@CU at different magnifications. Inset of (a) represents a high magnified view of CU.

the CU represents a 3D hierarchical structure with spikes and pores, resembling a natural sea urchin structure. Fig. 4b–e shows the growth of ZnO over the entire CU spikes. As illustrated in Fig. 4b and c, the ZnO 'kebabs' can be seen attached uniformly, and their growth was periodic along the axis of CU 'shish'. Further, Fig. 4d and e revealed that the ZnO 'kebabs' have an average thickness of *ca.*105 nm. This provides numerous pores and sites for multiple scattering, thereby attenuating incoming EM radiation.

The EDX patterns of ZnO@CU are recorded to analyze the elemental composition in the 3D construct, which is presented in Fig. 5. As depicted in Fig. 5, carbon, zinc and oxygen elements were present, confirming the presence of ZnO on CU surfaces. The weight percentage of ZnO in the ZnO@CU hybrid 3D construct was 56%, indicating its dense distribution over CU.

4.2. Healing properties of the ZCUP composite

The healing process of the scratched 2.0 ZCUP composite involved subjecting it to a temperature of 150 °C for a duration of 20 minutes. As illustrated in Fig. 6a–c, we can observe the evolution of scratch healing in the ZCUP composite over time. This remarkable healing capability is attributed to the presence of a di-sulfide dynamic covalent adaptive network within the polyetherimide (PEI) material. Earlier investigations have extensively reported that disulfide bonds, a key component of this network, exhibit a unique behavior under high-temperature conditions. They undergo cleavage when exposed to elev-

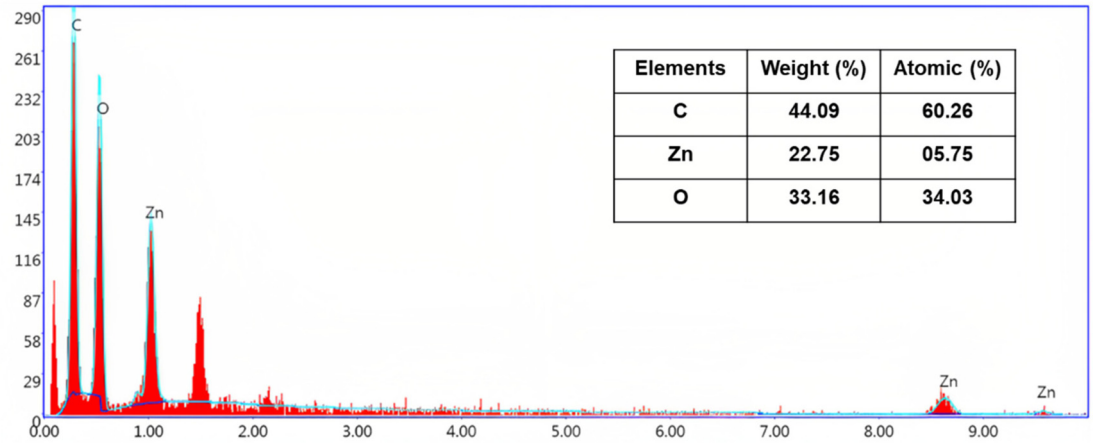

Elements	Weight (%)	Atomic (%)
C	44.09	60.26
Zn	22.75	05.75
O	33.16	34.03

Fig. 5 EDX pattern of ZnO@CU showing 55.91 weight percent of ZnO at a particular location in the hybrid construct.

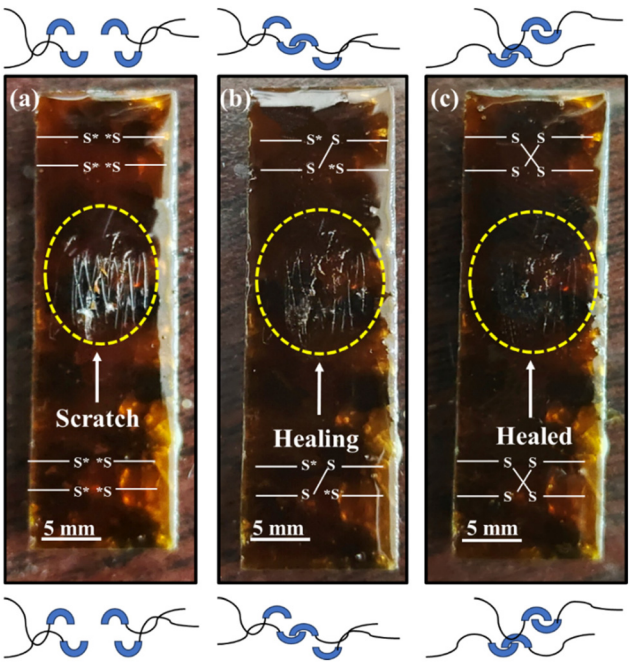

Fig. 6 Digital images of (a) scratched composite and healed composites after (b) 10 min and (c) 20 min.

ated temperatures and then reorganize themselves as the material cools down. This rearrangement of the network's topology during the cooling phase plays a pivotal role in the remarkable ability of the ZCUP composite to heal scratches, demonstrating the effectiveness of di-sulfide bonds in facilitating the material's self-healing properties.[41–44]

4.3. Charge transport in the composites

The electrical conductivity of the composite is vital and typically depends on the filler's intrinsic conductivity, junction resistance, amount, dispersion and distribution in the composites.[8,32] In this case, the ZnO@CU was dispersed in the PEI solution. In addition, the additional composite with only the PEI matrix is tested to highlight the substantial differences, which are presented in Fig. 7. The PEI matrix exhibits distinctive insulating properties, with discernible variations in conductivity across low- and high-frequency ranges. Specifically, the σ_{AC} of PEI is registered at 7.2×10^{-11} S cm^{-1} at 0.01 Hz. Notably, the introduction of designed fillers significantly enhances matrix σ_{AC}. The increase in conductivity is particularly evident with the inclusion of ZnO@CU (0–2 wt%) in the PEI matrix. Conductivity levels are observed to vary with the quantity of these additives. The mechanism governing conductivity in polymer nanocomposites is commonly attributed to either tunnelling or hopping. In the tunnelling mechanism, electrons traverse tunnels between non-contact particles, limiting their mobility and resulting in insulating behavior, such as that observed in PEI and electrons bound to move at high frequencies. In addition, in the low-frequency regime, the 0.1 ZCUP exhibits frequency independence, while in the high-frequency zone, it displays frequency-dependent behavior. In the

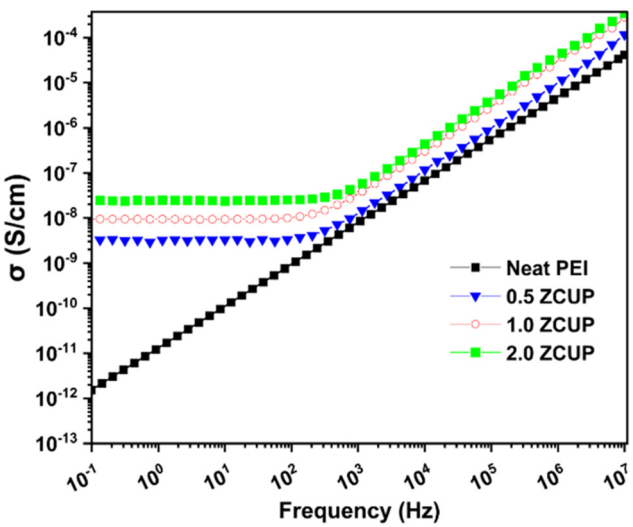

Fig. 7 AC electrical conductivity of the PEI and composites.

low-frequency regime, where fewer charges are present, electrons respond slowly to external electric fields. In contrast, in the high-frequency regime, electrons are compelled to align with the electric field direction, thereby enhancing conductivity. An alternative mode of electron transport occurs when fillers come into contact and form well-dispersed conductive pathways. The observed increase in conductivity values in ZnO@CU composites indicates the formation of a conductive network within the composite structure. Significantly, the 2.0 ZCUP composite achieves a conductivity of 4.5×10^{-4} S cm^{-1} at 0.01 Hz, a level of conductivity comparable to that of previously reported composites, which requires relatively higher filler loadings to reach this conductivity level.[23,52–54] These earlier reported composites, once they achieved this level of conductivity, demonstrated significant effectiveness in EMI shielding. Importantly, similar levels of AC conductivity are observed in ZnO@CU-filled PEI matrices, underscoring the influential role of CU in determining conductivity owing to the relatively low deposition of ZnO on CU. Overall, the conductive structure, comprising strategically designed large filler dimensions in close contact with one another, is expected to provide effective EMI shielding.

4.4. Mechanical robustness and thermal stability

The effect of ZnO@CU on the reinforcement of PEI composite is studied using DMA. Fig. 8a and b shows the DMA results of neat PEI and the composites. The storage modulus of the composite scales with an increasing amount of ZnO@C–U (Fig. 8a). At 2 wt% loading of ZnO@CU, a significant increase of 64% in the storage modulus was observed, followed by 44% for 1 wt% and 24% for 0.5 wt% of ZnO@C–U respectively. Additionally, a decrease in the tan δ peak values was observed with increasing wt% of ZnO@C–U (Fig. 8b). The storage modulus and tan δ values are summarized in Table 1.

The restrictions in the chain mobility of PEI due to the interaction between ZnO@CU and PEI lead to an increase in the storage modulus.[55,56] The 'shish-kebab' structure of ZnO leads to increased roughness and mechanical interlocking between PEI and individual ZnO@CU fibers, thereby increasing polymer–filler interaction. Additionally, the peroxide treatment, which led to –OH functionality in the carbon fiber prior to CU synthesis, facilitates polar interaction between ZnO@CU and PEI. The same mechanism holds true for the decrease in tan δ values. The tan δ values represent a viscous component of the viscoelastic material. The decrease in tan δ can be attributed to the increasing magnitude of the elastic component owing to the presence of ZnO@CU filler as reinforcement.

The thermal stability of the neat PEI and 2.0 ZCUP composites was measured using TGA (Fig. 9). TGA plots clearly show

Table 1 Storage modulus and tan δ values of ZnO@C–U/PEI composites

Sample	Storage modulus (MPa)@40 °C	tan δ
PEI	1759	2.09
0.5 ZCUP	2194	1.90
1 ZCUP	2534	1.56
2 ZCUP	2901	1.11

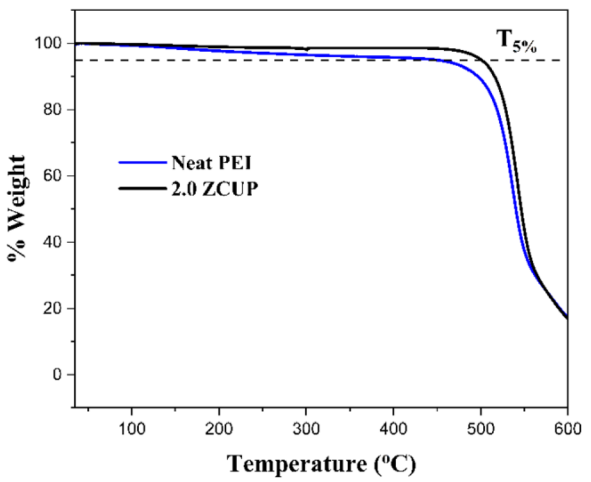

Fig. 9 TGA plots of neat PEI and 2.0 ZCUP.

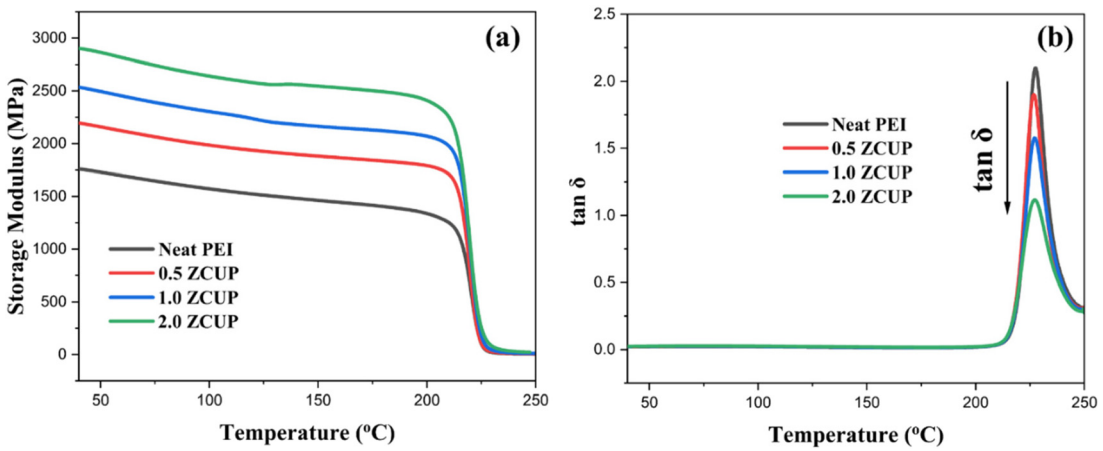

Fig. 8 DMA curves of ZnO@C–U/PEI composites (a): storage modulus *vs.* temperature; (b): tan δ *vs.* temperature.

a higher thermal stability of 2.0 ZCUP than neat PEI. The $T_{5\%}$ (the temperature at 5% degradation) of neat PEI and 2.0 ZCUP is 446 °C and 500 °C, respectively, clearly showing the effect of incorporation of ZnO@C–U in improving the thermal stability of PEI.[57]

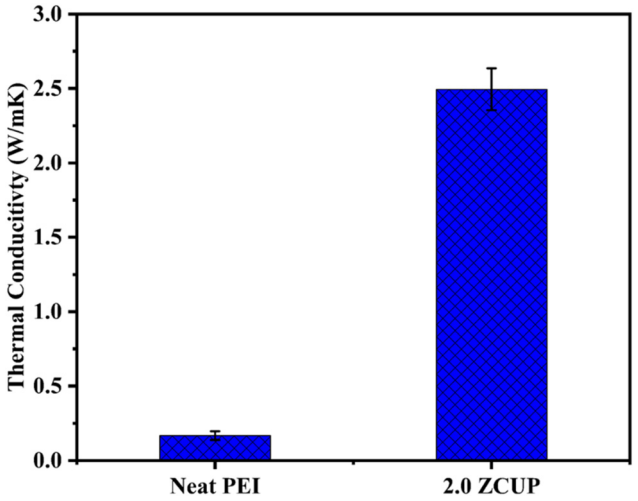

Fig. 10 Thermal conductivity of 2.0 ZCUP and PEI nanocomposites.

4.5. Thermal conductivity performance

The homogeneous dispersion and abundant interfaces of ZnO@CU within the PEI polymer matrix play a crucial role in establishing a highly thermally conductive network.[58] The SEM micrograph (Fig. 4) reveals that ZnO@CU exhibits numerous spikes, surfaces, and porosity, providing ample opportunities for PEI polymer molecules to generate additional interfacial forces. Consequently, ZnO@CU easily forms a continuous network within the PEI matrix, significantly contributing to the enhancement of thermal conductivity in this 3D construct. Comparatively, the thermal conductivity of the 2.0 ZCUP nanocomposites exhibited a notable increase when compared to the neat PEI composite. Specifically, the thermal conductivity of the 2.0 ZCUP reached 2.47 W (m K)$^{-1}$, a substantial improvement over the neat PEI sample, which demonstrates a thermal conductivity value of 0.33 W (m K)$^{-1}$ (Fig. 10).

4.6. EMI shielding performance

The EMI shielding performance of ZCUP composites is studied in the X-band, and their outcomes are depicted in Fig. 11a–c. As illustrated in Fig. 11a, it is obvious that the SE_T depends on the amount of ZnO@CU in the PEI composite. The highest SE_T value of −40.6 dB is obtained with the 2.0 ZCUP. This is attributed to the fact that composites with

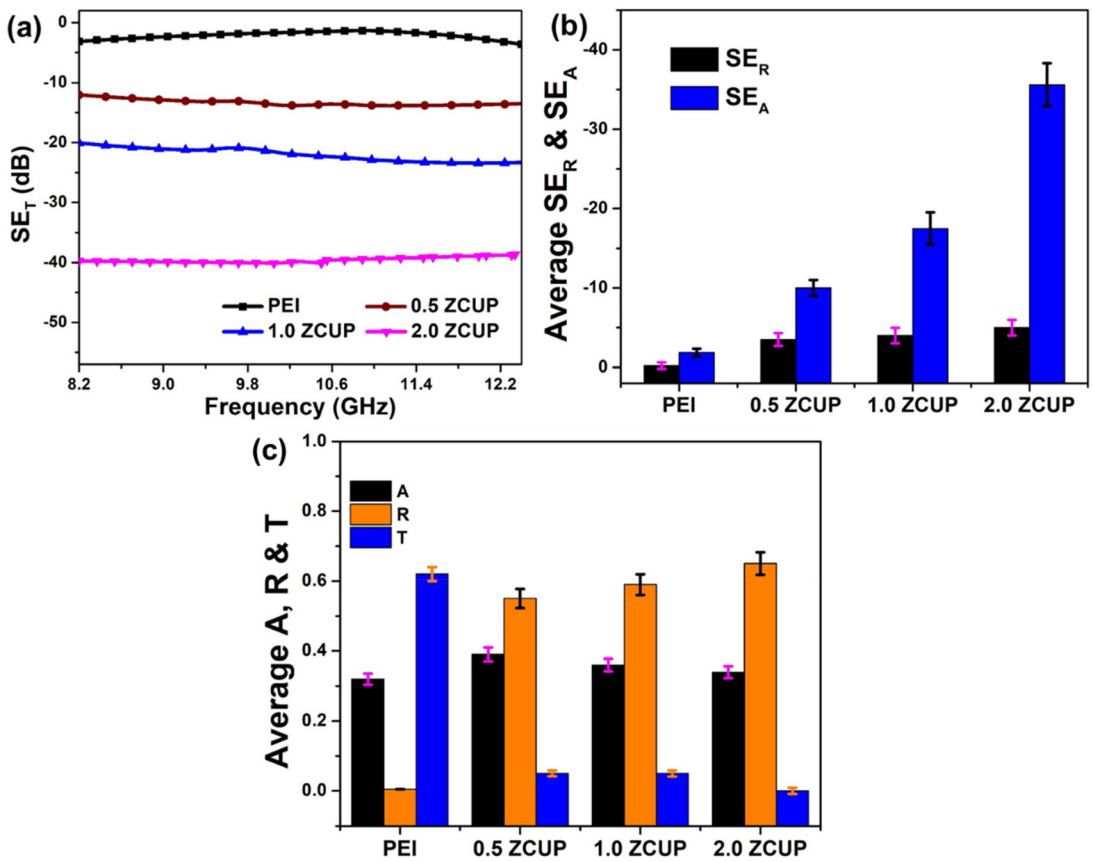

Fig. 11 (a) SE_T; (b) average SE_R–SE_A; and (c) *A*, *R*, and *T* of nanocomposites.

higher filler loading offer improved electrical interconnection within the PEI polymer matrix. Additionally, the micro-spikes, porous nature and the 'kebab'-like structures of ZnO@CU offer numerous interfaces between ZnO and CU, which collectively contribute to significantly enhanced EMI shielding performance.[1,18,35,51] The EMI shielding properties in terms of average absorption (SE_A) and reflection (SE_R) are shown in Fig. 10b. Observations reveal that SE_A has a greater contribution to total SE. Furthermore, to emphasize the effect of ZnO decoration on CU, we investigated the EMI shielding performance of a composite consisting of uncoated CU (2 wt%) in the PEI matrix (ESI†). Interestingly, the CU-filled composite exhibited a SE_T value of −33.8 dB (ESI, Fig. S1†). The SE_T of 2.0 ZCUP with similar loading conditions exhibited −40.6 dB. Thus, uncoated CU illustrates lower values compared to CU with ZnO coating. This significant difference in SE_T values can be attributed to the presence of ZnO with a flower structure creating multiple interfaces within the composite, which is complemented by the porous nature of the CU. These interfaces collectively contribute to a higher SE_T value of 2.0 ZCUP compared to the sample containing CU (2 wt%) in PEI. In addition, owing to the high dielectric constant of ZnO, it facilitates abundant polarization centres at CU surfaces and the formation of a capacitor between CU–ZnO–CU, CU–PEI–CU and ZnO–PEI–ZnO that combined to enhance EMI shielding significantly.

Further, to gain an inclusive understanding of how these composites deliver EMI shielding, we calculate the relationship between three key parameters: the transmission coefficient (T), absorption coefficient (A), and reflection coefficient (R). It is important to note that these power coefficients are commonly used to evaluate power distribution when EM waves interact with composites.[1,13,49–51] They provide a comprehensive assessment of the material's ability to transmit, absorb, and reflect EM waves. As shown in Fig. 11c, it is evident that the R values are significantly higher than the A values, indicating that shielding is primarily dominated by reflection. This is primarily owing to the relatively high conductivity of these samples, which leads to an impedance mismatch at the interface between the composite and air.[1,51] Consequently, there is a strong reflection of EM waves. The T values for these composites are considerably lower compared to the pristine PEI composite, approaching near-zero levels. This demonstrates the potential of these protectors to effectively block almost all incoming EM waves.

Further, the possible EMI shielding mechanism of the composite is proposed here. Fig. 12 depicts a cartoon of the shielding mechanism within the ZCUP composite. Owing to the high conductivity (CU dominating) of ZCUP, it leads to an impedance mismatch at the air-composite interface. Hence, the incoming EM waves are largely reflected at ZCUP composite surfaces upon contact, resulting in a reflection dominant mechanism. In addition, part of the incident wave managed to enter inside (A values in Fig. 11c). As the penetrating EM waves encounter the interior distribution of the composite, then the open-connected pores of ZnO@CU guide the EM waves to travel deep inside the composite. Hence, the wave that entered was attenuated within the ZnO@CU network and opened the pores of CU. Finally, the abundant open pores of CU significantly assist in effectively reducing EM wave strength. Hence, these waves are either absorbed or transformed into heat energy. In addition, the 'shish-kebab'-like morphology of ZnO

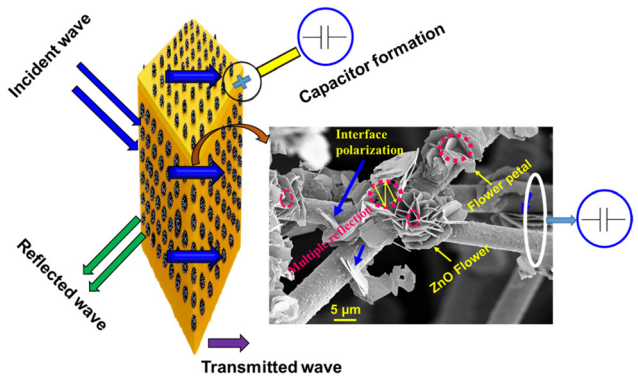

Fig. 12 Schematic of the EMI shielding mechanism in composites.

Table 2 Comparison of EMI shielding performance of the as-prepared composite with previously reported material systems

Filler	Matrix	Filler synthesis method	Filler (wt%)	Thickness (mm)	Max. SE_T (dB)	Ref.
CNT	PDMS	Solvothermal	2.2	2.5	47	59
CNT/CTAB	WPU	Freeze-drying	4.3	2	24.9	60
CNT/SiO_2	PI	Freeze casted, thermal imidization	45.0	9	110	61
Graphene sheets	PANI	Hydrothermal, microwave, freeze-dried	1.0	4.0	38.3	62
CNF–SCF/rGO	PI	CVD and freeze-drying	33.5	0.25	45.0	63
m-CNT	Aramid nanofiber aerogel	Wet spinning, freeze drying	60.0	0.9	30.0	64
MWCNT	PCL/PS blends	Melt blending	5.0	2.0	40.0	65
CNT	Starch	Mechanical blending	4.8	1.6	33.1	66
CU	Epoxy	Acid refluxing	23	1.0	52.0	50
CNF + Fe_3O_4 NP	PVDF + PMMA	Spray coating	80.0	0.5	60.0	67
ZnO@CU	PEI	Microwaves	2.0	2.0	40.6	This work

supported multiple scattering, resulting in extra attenuation. The interfacial polarization created at the boundaries between ZnO–CU also contributed to attenuating the EM waves significantly. In addition, with the addition of ZnO@CU to the PEI matrix, many capacitors were formed in the composite, such as ZnO–PEI–ZnO, CU–ZnO–CU and CU–PEI–CU. The enhanced number of capacitor formations is anticipated to improve the material's EMI shielding capability. Overall, it can be proposed that the shielding property of ZCUP improved owing to the high conductivity, shish kebab-type structure of ZnO, interfacial polarization and abundant open porous network structure of CU.

Further, Fig. 11a clearly shows that the SE_T relies strongly on the amount of filler material used. In addition, it is well recognised that the EMI shielding performance of composites typically depends on two key factors: the thickness of the material and the ratio of filler content. Therefore, we also aimed to create lightweight and thin composites that excel at blocking EMI while still maintaining high shielding performance. To justify the significance of our developed material, a comprehensive comparison is conducted between our developed composite and recently reported works in the field, as depicted in Table 2. The results clearly demonstrate the superiority of our composite across various aspects. First, when evaluating EMI shielding effectiveness, our composite outperformed the others with an impressive −40.6 dB SE_T value. This exceptional performance was achieved with just 2 wt% of ZnO@CU filler content in the PEI matrix at a thickness of 2.0 mm. Moreover, our work showcased significant advantages in terms of synthesis efficiency and cost effectiveness. We employed a novel and cost-effective microwave synthesis process to develop the filler material, which not only reduced expenses but also accelerated production rates, making it an attractive choice for large-scale manufacturing.[1] Additionally, the ZCUP composite exhibited 100% retention of EMI SE after the self-healing process. In conclusion, our developed composite stands as a remarkable alternative for EMI shielding applications. Its ability to deliver high performance with a thinner and lighter composition, coupled with the benefits of cost-effectiveness, efficient fabrication and self-healing, sets it apart from other recent works in the field.[30,31,36,49,50]

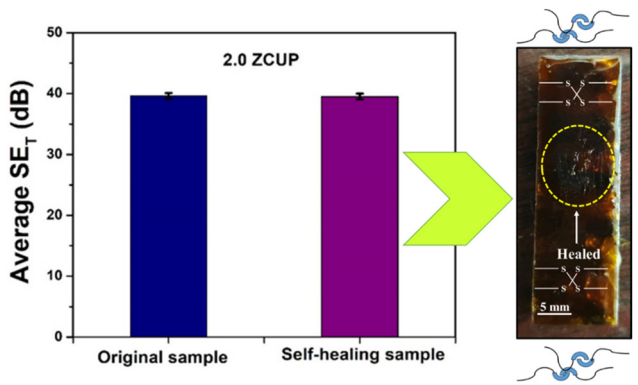

Fig. 13 The effect of self-healing on SE_T values.

Self-healing is another substantial feature that extends the service life of the EMI shielding material.[37,39,40] Hence, to explore the qualitative assessment of self-healing, the variations in EMI shielding performance were recorded before and after the healing process (Fig. 13). As shown in Fig. 13, the EMI SE_T of the 2.0 ZCUP exhibits excellent stability during the healing cycles. When the composite was partially damaged, a noticeable 20% decrease in EMI SE was observed. However, after a heat treatment of 2.0 ZCUP, the EMI SE approached its original values, indicating 100.0% retention. During the self-healing process, the polymer molecular chains intricately reconnected, while at the interface, the ZnO@CU network underwent rejuvenation. This molecular rearrangement is responsible for the remarkable, consistent recovery of the EMI shielding performance in the 2.0 ZCUP composite, even after undergoing several instances of damage at the same location.

To understand its practical utility, we utilized a Bluetooth module (HC-05) to analyze real-time shielding performance. The module was connected to a mobile phone using an Android application, as illustrated in Fig. 14. Initially, the paired connec-

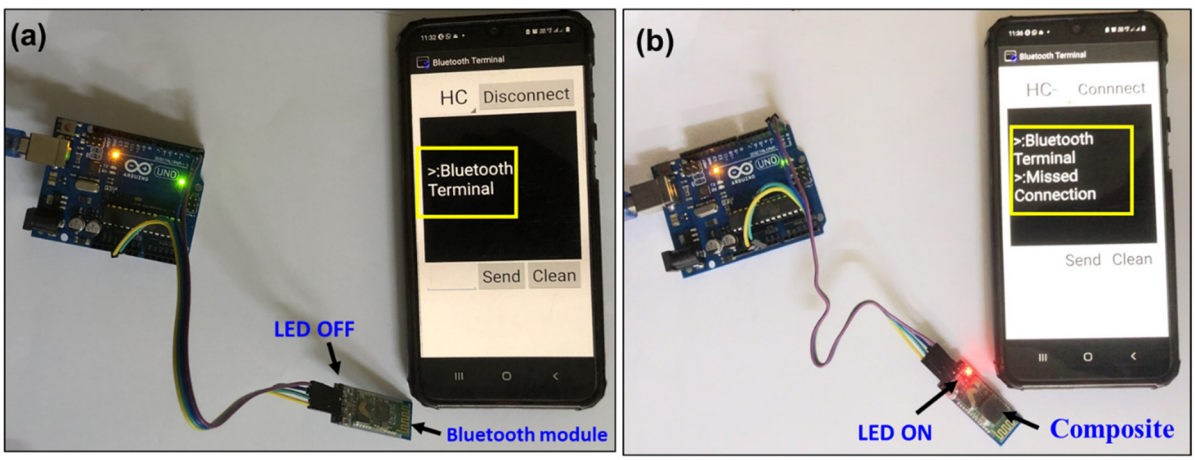

Fig. 14 Two states of Bluetooth module and mobile phone: (a) connected and (b) disconnected.

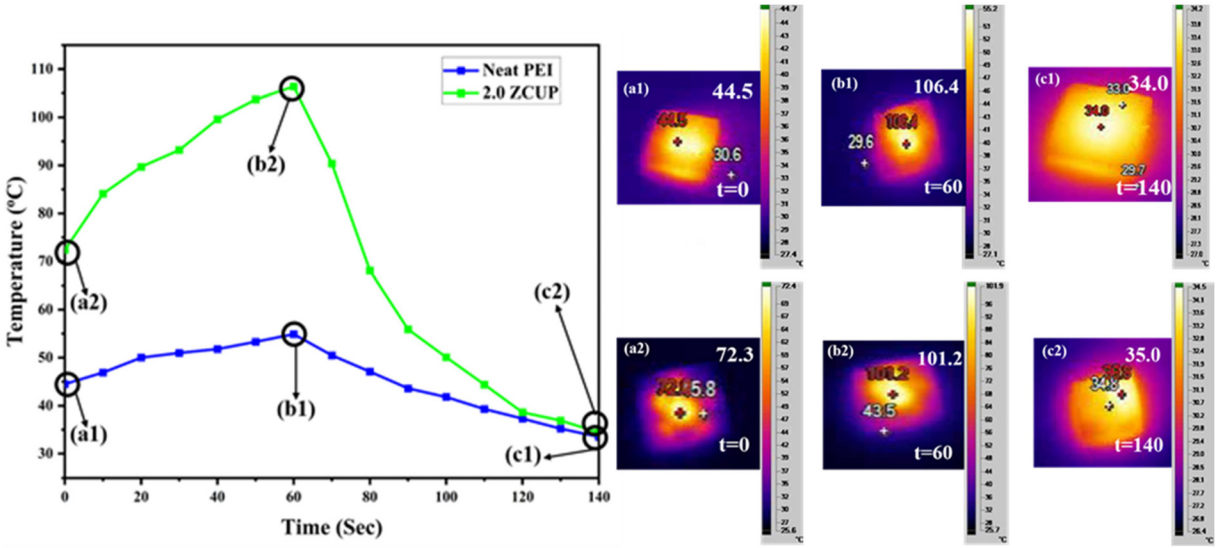

Fig. 15 Temperature variation in the 2.0 ZCUP composite as a function of heating and cooling.

tion between the phone and Bluetooth module exhibited a robust signal in the mobile Android application (Fig. 14a). However, when we placed the proposed composite on the module, we observed a complete loss of the signal, indicating disconnection of the module (Fig. 14b). These findings highlight the capability of the designed materials to shield effectively against undesired electromagnetic (EM) radiation. Consequently, the developed nanocomposite has immense potential to safeguard the real world from EMI pollutants that arise from the competitive market of telecommunication industries.

4.7. Heat dissipation study

Heat dissipation is essential for EMI shielding materials in practical use.[1,13,68] Hence, a qualitative assessment is conducted to examine the heat dissipation capability of our newly developed composite. For this, a 2 mm thick 2.0 ZCUP sample was heated with a laser for 60 s, and temperature changes were recorded at 10 s intervals. The sample was then allowed to cool for the next 60 s after turning off the laser, and temperature variation was further noted, as illustrated in Fig. 15. The 2.0 ZCUP composite reached 105 °C in 60 seconds and rapidly returned to its initial temperature after turning off the laser, indicating its potential to rapidly handle real-world heat situations.

5. Conclusions

In summary, the facile microwave synthesis method successfully produced ZnO-decorated CU 3D constructs within just 120 seconds using a power level of 300 W. SEM analysis unveiled a flower-like ZnO morphology arranged periodically across CU surfaces, resembling a shish kebab structure. Incorporating 2 wt% of ZnO@CU into a PEI composite led to a remarkable −40.6 dB shielding efficiency at a 2 mm thickness in the X-band. Notably, this EMI shielding efficiency endured even after self-healing procedures. The dominant EMI shielding behaviour was attributed to reflection, primarily resulting from the altered conductivity owing to ZnO@CU integration. The ZnO flowers on CU facilitated multiple scattering and polarization, enhancing EMI shielding performance even with lower filler contents. Additionally, the composites exhibited substantial enhancements in mechanical and thermal properties compared to the pure PEI composite.

Conflicts of interest

There are no conflicts to declare.

Acknowledgements

This work was financially supported by the D. S. Kothari postdoctoral grant of the Ministry of Science and Technology of India (Grant No. 202122-EN/20-21/0067).

References

1 S. K. Singh, K. Sushmita, D. Sharma, Y. O. Waidi and S. Bose, Aerogels containing ionomers and microwave assisted growth of carbon nanostructures on carbon urchins for multifunctional electromagnetic interference shielding, *Carbon*, 2023, **209**, 118036, DOI: 10.1016/j.carbon.2023.118036.

2 A. K. Singh, A. Kumar, A. Srivastava, A. N. Yadav, K. Haldar, V. Gupta and K. Singh, Lightweight reduced graphene oxide-ZnO nanocomposite for enhanced dielectric loss and excellent electromagnetic interference shielding, *Composites, Part B*, 2019, **172**, 234–242, DOI: 10.1016/j.compositesb.2019.05.062.

3 M. A. Morales, T. C. Henry and L. G. Salamanca-Riba, Model of electromagnetic interference shielding effectiveness for a multifunctional composite containing carbon-fiber-reinforced polymer and copper mesh layers, *Carbon*, 2023, **212**, 118179, DOI: **10.1016/j.carbon.2023.118179**.
4 Z. Barani, F. Kargar, Y. Ghafouri, S. Ghosh, K. Godziszewski, S. Baraghani, Y. Yashchyshyn, G. Cywiński, S. Rumyantsev, T. T. Salguero and A. A. Balandin, Electrically Insulating Flexible Films with Quasi–1D van der Waals Fillers as Efficient Electromagnetic Shields in the GHz and Sub–THz Frequency Bands, *Adv. Mater.*, 2021, **33**, 2007286, DOI: **10.1002/adma.202007286**.
5 P. Yang, M. Dai, H. Xiong, S. Hao, W. Zhang, B. Zhang, C. Ouyang, Q. Li, F. He, J. Miao and X. Wu, 3D Nickel Skeletons as Ultrabroadband Terahertz Absorbers, *Adv. Electron. Mater.*, 2021, **7**, 2100626, DOI: **10.1002/aelm.202100626**.
6 M. S. Irfan, M. A. Ali, T. Khan, S. Anwer, K. Liao and R. Umer, MXene and graphene coated multifunctional fiber reinforced aerospace composites with sensing and EMI shielding abilities, *Composites, Part A*, 2023, **165**, 107351, DOI: **10.1016/j.compositesa.2022.107351**.
7 B. Zhao, Y. Du, Z. Yan, L. Rao, G. Chen, M. Yuan, L. Yang, J. Zhang and R. Che, Structural Defects in Phase–Regulated High–Entropy Oxides toward Superior Microwave Absorption Properties, *Adv. Funct. Mater.*, 2023, **33**, 2209924, DOI: **10.1002/adfm.202209924**.
8 B. Zhao, Z. Yan, Y. Du, L. Rao, G. Chen, Y. Wu, L. Yang, J. Zhang, L. Wu, D. W. Zhang and R. Che, High–Entropy Enhanced Microwave Attenuation in Titanate Perovskites, *Adv. Mater.*, 2023, **35**, 2210243, DOI: **10.1002/adma.202210243**.
9 C. Wen, X. Li, R. Zhang, C. Xu, W. You, Z. Liu, B. Zhao and R. Che, High-Density Anisotropy Magnetism Enhanced Microwave Absorption Performance in $Ti_3C_2T_x$ MXene@Ni Microspheres, *ACS Nano*, 2022, **16**, 1150–1159, DOI: **10.1021/acsnano.1c08957**.
10 B. Zhao, Z. Bai, H. Lv, Z. Yan, Y. Du, X. Guo, J. Zhang, L. Wu, J. Deng, D. W. Zhang and R. Che, Self-Healing Liquid Metal Magnetic Hydrogels for Smart Feedback Sensors and High-Performance Electromagnetic Shielding, *Nano-Micro Lett.*, 2023, **15**, 79, DOI: **10.1007/s40820-023-01043-3**.
11 A. Sharma, R. Kumar, A. Gupta, P. R. Agrawal, N. Dwivedi, D. P. Mondal, A. K. Srivastava and S. R. Dhakate, Enhanced electromagnetic interference shielding properties of phenolic resin derived lightweight carbon foam decorated with electrospun zinc oxide nanofibers, *Mater. Today Commun.*, 2022, **30**, 103055, DOI: **10.1016/j.mtcomm.2021.103055**.
12 D. M. Nivedhitha and S. Jeyanthi, Polyvinylidene fluoride—An advanced smart polymer for electromagnetic interference shielding applications—A novel review, *Polym. Adv. Technol.*, 2023, **34**, 1781–1806, DOI: **10.1002/pat.6015**.
13 M. P. Vidyashree, K. Sushmita, P. Nagarajan, M. K. Kokila and S. Bose, Mimicking 'sea-urchin' like heirarchical carbon structures self-assembled from carbon fibers for green EMI shielding, *Chem. Eng. J. Adv.*, 2023, **13**, 100430, DOI: **10.1016/j.ceja.2022.100430**.
14 Y. Du, Z. Yan, W. You, Q. Men, G. Chen, X. Lv, Y. Wu, K. Luo, B. Zhao, J. Zhang and R. Che, Balancing MXene Surface Termination and Interlayer Spacing Enables Superior Microwave Absorption, *Adv. Funct. Mater.*, 2023, **33**, 2301449, DOI: **10.1002/adfm.202301449**.
15 B. Zhao, Y. Du, H. Lv, Z. Yan, H. Jian, G. Chen, Y. Wu, B. Fan, J. Zhang, L. Wu, D. W. Zhang and R. Che, Liquid–Metal–Assisted Programmed Galvanic Engineering of Core–shell Nanohybrids for Microwave Absorption, *Adv. Funct. Mater.*, 2023, **33**, 2302172, DOI: **10.1002/adfm.202302172**.
16 B. Zhao, Y. Li, Q. Zeng, L. Wang, J. Ding, R. Zhang and R. Che, Galvanic Replacement Reaction Involving Core–Shell Magnetic Chains and Orientation–Tunable Microwave Absorption Properties, *Small*, 2020, **16**, 2003502, DOI: **10.1002/smll.202003502**.
17 E. Erfanian, R. Moaref, R. Ajdary, K. C. Tam, O. J. Rojas, M. Kamkar and U. Sundararaj, Electrochemically synthesized graphene/TEMPO-oxidized cellulose nanofibrils hydrogels: Highly conductive green inks for 3D printing of robust structured EMI shielding aerogels, *Carbon*, 2023, **210**, 118037, DOI: **10.1016/j.carbon.2023.118037**.
18 L. Mohan, T. N. Kumar, S. Karakkad and S. T. Krishnan, Development of Cost-Effective Carbon Nanofiber Epoxy Nanocomposites for Lightweight Wideband EMI Shielding Application, *IEEE Trans. Nanotechnol.*, 2021, **20**, 627–634, DOI: **10.1109/TNANO.2021.3103955**.
19 S. Raji, G. K. Sharma, B. R. Aranya and K. Prabhakaran, Carbon composite foams from the wasted banana leaf for EMI shielding and thermal insulation, *Carbon*, 2023, **213**, 118259, DOI: **10.1016/j.carbon.2023.118259**.
20 Z. Guo, P. Ren, F. Yang, T. Wu, L. Zhang, Z. Chen, S. Huang and F. Ren, MOF-Derived Co/C and MXene *co* -Decorated Cellulose-Derived Hybrid Carbon Aerogel with a Multi-Interface Architecture toward Absorption-Dominated Ultra-Efficient Electromagnetic Interference Shielding, *ACS Appl. Mater. Interfaces*, 2023, **15**, 7308–7318, DOI: **10.1021/acsami.2c22447**.
21 B. Wu, G. Qian, Y. Yan, M. M. Alam, R. Xia and J. Qian, Design of Interconnected Carbon Fiber Thermal Management Composites with Effective EMI Shielding Activity, *ACS Appl. Mater. Interfaces*, 2022, **14**, 49082–49093, DOI: **10.1021/acsami.2c13433**.
22 G. Lin, T. Zhou, Z. Zhou and W. Sun, Laser induced graphene for EMI shielding and ballistic impact damage detection in basalt fiber reinforced composites, *Compos. Sci. Technol.*, 2023, **242**, 110182, DOI: **10.1016/j.compscitech.2023.110182**.
23 B. Ucpinar Durmaz, A. O. Salman and A. Aytac, Electromagnetic Interference Shielding Performances of Carbon-Fiber-Reinforced PA11/PLA Composites in the X-Band Frequency Range, *ACS Omega*, 2023, **8**, 22762–22773, DOI: **10.1021/acsomega.3c01656**.
24 L. Lu, D. Xing, K. S. Teh, H. Liu, Y. Xie, X. Liu and Y. Tang, Structural effects in a composite nonwoven fabric on EMI shielding, *Mater. Des.*, 2017, **120**, 354–362, DOI: **10.1016/j.matdes.2017.02.025**.

25 X.-X. Wang, Q. Zheng, Y.-J. Zheng and M.-S. Cao, Green EMI shielding: Dielectric/magnetic "genes" and design philosophy, *Carbon*, 2023, **206**, 124–141, DOI: 10.1016/j.carbon.2023.02.012.

26 G. P. Abhilash, K. Sushmita, S. Bose and C. Shivakumara, Functionalization of dielectric BaTiO3 and semiconducting ZnO nanoparticles on rGO layers and their polymer composites: Applications in EMI shielding, *Synth. Met.*, 2023, **297**, 117387, DOI: 10.1016/j.synthmet.2023.117387.

27 D. Kuang, L. Liu, J. L. Mead, L. Deng, H. Luo and S. Wang, Facile synthesis and excellent microwave absorption performance of ultra-small ZnO-doped onion-like carbon nanoparticles, *Mater. Res. Bull.*, 2023, **157**, 112007, DOI: 10.1016/j.materresbull.2022.112007.

28 S. Palsaniya and S. Mukherji, Enhanced dielectric and electrostatic energy density of electronic conductive organic-metal oxide frameworks at ultra-high frequency, *Carbon*, 2022, **196**, 749–762, DOI: 10.1016/j.carbon.2022.05.042.

29 A. Shayesteh Zeraati and U. Sundararaj, Carbon nanotube/ZnO nanowire/polyvinylidene fluoride hybrid nanocomposites for enhanced electromagnetic interference shielding, *Can. J. Chem. Eng.*, 2020, **98**, 1036–1046, DOI: 10.1002/cjce.23717.

30 G. Hong, Q. Qu, O. J. Rojas, L. Li, D. Xie and Y. Liu, Epiphyte-inspired multifunctional biocomposites for electromagnetic interference shielding, *Chem. Eng. J.*, 2023, **469**, 143960, DOI: 10.1016/j.cej.2023.143960.

31 M. Han, X. Yin, S. Ren, W. Duan, L. Zhang and L. Cheng, Core/shell structured C/ZnO nanoparticles composites for effective electromagnetic wave absorption, *RSC Adv.*, 2016, **6**, 6467–6474, DOI: 10.1039/C5RA25295D.

32 A. Devaraju, P. Sivasamy and G. B. Loganathan, Mechanical properties of polymer composites with ZnO nano-particle, *Mater. Today: Proc.*, 2020, **22**, 531–534, DOI: 10.1016/j.matpr.2019.08.146.

33 R. Sathish Kumar, V. Vandhana Devi, D. M. Nivedhitha, S. Srish Satya, S. Visakan, S. Bharath Sharma and S. B. Sathish Kumar, Effect of nanoparticles in natural fiber reinforced polymer composites, *Mater. Today: Proc.*, 2023, S2214785323020266, DOI: 10.1016/j.matpr.2023.04.130.

34 J. Pavličević, M. Špírková, O. Bera, M. Jovičić, B. Pilić, S. Baloš and J. Budinski-Simendić, The influence of ZnO nanoparticles on thermal and mechanical behavior of polycarbonate-based polyurethane composites, *Composites, Part B*, 2014, **60**, 673–679, DOI: 10.1016/j.compositesb.2014.01.016.

35 D. Vaishnav and R. K. Goyal, Thermal and Dielectric Properties of High Performance Polymer/ZnO Nanocomposites, *IOP Conf. Ser.: Mater. Sci. Eng.*, 2014, **64**, 012016, DOI: 10.1088/1757-899X/64/1/012016.

36 Y. Lu, X. Xie, W. Wang, X. Qi, Y. Lei, J. Yang and Y. Wang, ZnO nanoparticles-tailored GO dispersion toward flexible dielectric composites with high relative permittivity, low dielectric loss and high breakdown strength, *Composites, Part A*, 2019, **124**, 105489, DOI: 10.1016/j.compositesa.2019.105489.

37 T. Wang, W.-C. Yu, C.-G. Zhou, W.-J. Sun, Y.-P. Zhang, L.-C. Jia, J.-F. Gao, K. Dai, D.-X. Yan and Z.-M. Li, Self-healing and flexible carbon nanotube/polyurethane composite for efficient electromagnetic interference shielding, *Composites, Part B*, 2020, **193**, 108015, DOI: 10.1016/j.compositesb.2020.108015.

38 Y.-H. Lee, L.-Y. Wang, C.-Y. Tsai and C.-W. Lee, Self-Healing Nanocomposites with Carbon Nanotube/Graphene/Fe_3O_4 Nanoparticle Tricontinuous Networks for Electromagnetic Radiation Shielding, *ACS Appl. Nano Mater.*, 2022, **5**, 16423–16439, DOI: 10.1021/acsanm.2c03492.

39 Z. Xie, Y. Cai, Z. Wei, Y. Zhan, Y. Meng, Y. Li, Y. Li, Q. Xie and H. Xia, Robust and self-healing polydimethylsiloxane/carbon nanotube foams for electromagnetic interference shielding and thermal insulation, *Compos. Commun.*, 2022, **35**, 101323, DOI: 10.1016/j.coco.2022.101323.

40 H. J. Sim, D. W. Lee, H. Kim, Y. Jang, G. M. Spinks, S. Gambhir, D. L. Officer, G. G. Wallace and S. J. Kim, Self-healing graphene oxide-based composite for electromagnetic interference shielding, *Carbon*, 2019, **155**, 499–505, DOI: 10.1016/j.carbon.2019.08.073.

41 H. Guo, Y. Han, W. Zhao, J. Yang and L. Zhang, Universally autonomous self-healing elastomer with high stretchability, *Nat. Commun.*, 2020, **11**, 2037, DOI: 10.1038/s41467-020-15949-8.

42 F. Ji, X. Liu, D. Sheng and Y. Yang, Epoxy-vitrimer composites based on exchangeable aromatic disulfide bonds: Reprocessibility, adhesive, multi-shape memory effect, *Polymer*, 2020, **197**, 122514, DOI: 10.1016/j.polymer.2020.122514.

43 A. Ruiz De Luzuriaga, R. Martin, N. Markaide, A. Rekondo, G. Cabañero, J. Rodríguez and I. Odriozola, Epoxy resin with exchangeable disulfide crosslinks to obtain reprocessable, repairable and recyclable fiber-reinforced thermoset composites, *Mater. Horiz.*, 2016, **3**, 241–247, DOI: 10.1039/C6MH00029K.

44 B. Wan, X. Dong, X. Yang, M.-S. Zheng, G. Chen and J.-W. Zha, High strength, stable and self-healing copolyimide for defects induced by mechanical and electrical damages, *J. Mater. Chem. C*, 2022, **10**, 11307–11315, DOI: 10.1039/D2TC01605B.

45 P. Banerjee, R. Raj, S. Kumar and S. Bose, Tuneable chemistry at the interface and self-healing towards improving structural properties of carbon fiber laminates: a critical review, *Nanoscale Adv.*, 2021, **3**, 5745–5776, DOI: 10.1039/D1NA00294E.

46 P. Das, A. Katheria, J. Nayak, S. Das, K. Nath, S. K. Ghosh, K. Naskar and N. Ch, Das, Facile preparation of self-healable and recyclable multilayered graphene-based nanocomposites for electromagnetic interference shielding applications, *Colloids Surf., A*, 2023, **676**, 132244, DOI: 10.1016/j.colsurfa.2023.132244.

47 K. Kong, B. K. Deka, S. K. Kwak, A. Oh, H. Kim, Y.-B. Park and H. W. Park, Processing and mechanical characterization of ZnO/polyester woven carbon–fiber composites with different ZnO concentrations, *Composites, Part A*, 2013, **55**, 152–160, DOI: 10.1016/j.compositesa.2013.08.013.

48 D. Luo, J. Fei, C. Zhang, H. Li, L. Zhang and J. Huang, Optimization of mechanical and tribological properties of carbon fabric/resin composites via controlling ZnO nanorods morphology, *Ceram. Int.*, 2018, **44**, 15393–15401, DOI: **10.1016/j.ceramint.2018.05.191**.

49 B. Wang, Y. Duan and J. Zhang, A controllable interface performance through varying ZnO nanowires dimensions on the carbon fibers, *Appl. Surf. Sci.*, 2016, **389**, 96–102, DOI: **10.1016/j.apsusc.2016.07.092**.

50 M. P. Vidyashree, K. Sushmita, M. K. Kokila and S. Bose, 'Template-free' synthesis of self-assembled micro-spikes resulting in 'sea-urchin'-like carbon structures for suppressing electromagnetic radiation, *Mater. Adv.*, 2022, **3**, 7618–7631, DOI: **10.1039/D2MA00715K**.

51 S. K. Singh, M. J. Akhtar and K. K. Kar, Hierarchical Carbon Nanotube-Coated Carbon Fiber: Ultra Lightweight, Thin, and Highly Efficient Microwave Absorber, *ACS Appl. Mater. Interfaces*, 2018, **10**, 24816–24828, DOI: **10.1021/acsami.8b06673**.

52 J. Hong, J. Kwon, D. Im, J. Ko, C. Y. Nam, H. G. Yang, S. H. Shin, S. M. Hong, S. S. Hwang, H. G. Yoon and A. S. Lee, Best practices for correlating electrical conductivity with broadband EMI shielding in binary filler-based conducting polymer composites, *Chem. Eng. J.*, 2023, **455**, 140528, DOI: **10.1016/j.cej.2022.140528**.

53 M. F. Shakir, A. N. Khan, R. Khan, S. Javed, A. Tariq, M. Azeem, A. Riaz, A. Shafqat, H. M. Cheema, M. A. Akram, I. Ahmad and R. Jan, EMI shielding properties of polymer blends with inclusion of graphene nano platelets, *Results Phys.*, 2019, **14**, 102365, DOI: **10.1016/j.rinp.2019.102365**.

54 M. Mahmoodi, M. Arjmand, U. Sundararaj and S. Park, The electrical conductivity and electromagnetic interference shielding of injection molded multi-walled carbon nanotube/polystyrene composites, *Carbon*, 2012, **50**, 1455–1464, DOI: **10.1016/j.carbon.2011.11.004**.

55 D. Kaushik, S. Gairola, B. Varikkadinmel and I. Singh, Static and dynamic mechanical behavior of intra–hybrid jute/sisal and flax/kenaf reinforced polypropylene composites, *Polym. Compos.*, 2023, **44**, 515–523, DOI: **10.1002/pc.27114**.

56 H. Jena, A. Panigrahi and M. Jena, Mechanical property of jute fibre reinforced polymer composite filled with clam shell filler: a marine waste, *Adv. Mater. Process. Technol.*, 2023, **9**, 75–91, DOI: **10.1080/2374068X.2022.2085387**.

57 P. Vasanthkumar, R. Balasundaram, N. Senthilkumar, K. Palanikumar, K. Lenin and B. Deepanraj, Thermal and thermo-mechanical studies on seashell incorporated Nylon-6 polymer composites, *J. Mater. Res. Technol.*, 2022, **21**, 3154–3168, DOI: **10.1016/j.jmrt.2022.10.117**.

58 X. Wang, W. Li, Z. Zhang, K. Chen and W. Gan, Selective localization of multi–walled carbon nanotubes in epoxy/polyetherimide system and properties of the conductive composites, *J. Appl. Polym. Sci.*, 2019, **136**, 47911, DOI: **10.1002/app.47911**.

59 R.-Y. Ma, S.-Q. Yi, J. Li, J.-L. Zhang, W.-J. Sun, L.-C. Jia, D.-X. Yan and Z.-M. Li, Highly efficient electromagnetic interference shielding and superior mechanical performance of carbon nanotube/polydimethylsiloxane composite with interface-reinforced segregated structure, *Compos. Sci. Technol.*, 2023, **232**, 109874, DOI: **10.1016/j.compscitech.2022.109874**.

60 Y. Zhan, F. Liu, Y. Cai, L. Man, Y. Li, Y. Meng, H. Xia and Z. Chen, EMI shielding, thermal and antibacterial performances of ecofriendly castor oil–based waterborne polyurethane favored by combining carbon nanotube and cetyltrimethylammonium bromide, *Ind. Crops Prod.*, 2023, **202**, 117060, DOI: **10.1016/j.indcrop.2023.117060**.

61 J. He, M. Han, K. Wen, C. Liu, W. Zhang, Y. Liu, X. Su, C. Zhang and C. Liang, Absorption-dominated electromagnetic interference shielding assembled composites based on modular design with infrared camouflage and response switching, *Compos. Sci. Technol.*, 2023, **231**, 109799, DOI: **10.1016/j.compscitech.2022.109799**.

62 L. Wang, H. Li, S. Xiao, M. Zhu and J. Yang, Preparation of p-Phenylenediamine Modified Graphene Foam/Polyaniline@Epoxy Composite with Superior Thermal and EMI Shielding Performance, *Polymers*, 2021, **13**, 2324, DOI: **10.3390/polym13142324**.

63 Z. Wu, J. Dong, X. Li, X. Zhao, W. Tan, C. Ji and Q. Zhang, Tough polyimide composites synergistically reinforced by carbon nanofiber-grafted carbon fiber and rGO for improved heat dissipation and electromagnetic interference shielding, *J. Mater. Sci. Technol.*, 2023, **149**, 225–236, DOI: **10.1016/j.jmst.2022.11.039**.

64 M. Li, X. Chen, X. Li, J. Dong, C. Teng, X. Zhao and Q. Zhang, Ultralight aerogel textiles based on aramid nanofibers composites with excellent thermal insulation and electromagnetic shielding properties, *Compos. Commun.*, 2022, **35**, 101346, DOI: **10.1016/j.coco.2022.101346**.

65 F. Zou, X. Liao, C. Lv, F. Guo, S. Shi, X. Wang and G. Li, Supercritical carbon dioxide assisted phase coarsening of double-percolated polycaprolactone/polystyrene/multi-wall carbon nanotube composites for improved electrical performance and electromagnetic interference shielding, *J. Supercrit. Fluids*, 2023, **199**, 105961, DOI: **10.1016/j.supflu.2023.105961**.

66 X. Mei, Y. Zhao, H. Jiang, T. Gao, Z. Huang and J. Qu, Multifunctional starch/carbon nanotube composites with segregated structure: Electrical conductivity, electromagnetic interference shielding effectiveness, thermal conductivity, and electro–thermal conversion, *J. Appl. Polym. Sci.*, 2023, **140**, e53904, DOI: **10.1002/app.53904**.

67 N. Arooj, T. M. Khan, M. Mumtaz, A. Rehman, I. Ahmad, A. Shah, M. U. Hassan and M. Raffi, Polymeric Fe_3O_4 Nanoparticle/Carbon Nanofiber Hybrid Nanocomposite Coatings for Improved Terahertz Shielding, *ACS Appl. Nano Mater.*, 2023, **6**, 5264–5273, DOI: **10.1021/acsanm.2c05313**.

68 S. Parasuram, P. Banerjee, R. Raj, S. Kumar and S. Bose, Electrophoretically Deposited Multiscale Graphene Oxide/Carbon Nanotube Construct Mediated Interfacial Engineering in Carbon Fiber Epoxy Composites, *ACS Appl. Mater. Interfaces*, 2023, **15**, 28581–28593, DOI: **10.1021/acsami.3c04538**.

